Geophys. J. Int. (2007) **169,** 100–112 doi: 10.1111/j.1365-246X.2006.03308.x

Microseismicity of the ultraslow-spreading Gakkel ridge, Arctic Ocean: a pilot study

Vera Schlindwein,[1] Christian Müller[1,2] and Wilfried Jokat[1]

[1] *Alfred Wegener Institute for Polar and Marine Research, Am alten Hafen* 26, D-27568 *Bremerhaven, Germany. E-mail: Vera.Schlindwein@awi.de*
[2] *FIELAX GmbH, Schifferstr.* 10-14, D-27568 *Bremerhaven, Germany*

Accepted 2006 November 20. Received 2006 November 20; in original form 2006 March 13

SUMMARY

The active mid-ocean ridge of the Arctic Ocean, named Gakkel ridge, is the slowest spreading ridge of the global system of mid-oceanic ridges with full spreading rates declining from about 12.5 to 6 mm yr^{-1} from west to east. Geological models of seafloor spreading predict a decreasing intensity of magmatic processes with decreasing spreading rate. In summer 2001, the multidisciplinary Arctic Mid-Ocean Ridge Expedition (AMORE2001) discovered robust magmatism at western Gakkel ridge, an amagmatic section further east and pronounced volcanic centres at eastern Gakkel ridge. During AMORE2001, an attempt was made at recording the microearthquake activity of the ridge which allows important insights into the character and dynamics of active crustal accretion at the ridge axis. Due to the permanent ice cover of the Arctic Ocean, the use of ocean-bottom seismometers bears the risk of instrument and data loss. In this pilot study, we used for the first time drifting ice floes as platforms for small seismological arrays. The arrays consisted of four three-component seismometers equipped with GPS devices and arranged as a triangle with a central seismometer and a side length of about 1 km. Three such arrays were deployed in different rift segments and recorded the seismic activity continuously for 5–11 days at a sampling rate of 100 Hz. The array technique allowed to distinguish clearly between icequakes and earthquakes and to localize the earthquake source to within few kilometres or less depending on epicentral distance. We intensively discuss the detection capabilities and the location accuracy of this single array on a drifting ice floe. Earthquake magnitudes could not be calculated in our pilot study but are estimated to be significantly smaller than magnitude 2 by comparison with a regional earthquake of known magnitude. Furthermore, we analyse the characteristics of the recorded seismic events ranging from long waveforms of regional events to short local events with reverberations in the water column. All of the arrays recorded numerous microearthquakes in the central rift valley and on its flanks which we interpret as tectonic earthquakes. A swarm of microearthquakes was localized with high accuracy underneath the crest of a volcanic ridge in the rift valley and is proposed to have magmatic origin. The pilot study was thus successful in detecting, localizing and interpreting microearthquakes below magnitude 2 at Gakkel ridge. However, we suggest improvements of the method for a comprehensive microearthquake survey of Gakkel ridge which should aim at an understanding of active magmatism and faulting at ultraslow-spreading ridges.

Key words: earthquake location, microseismicity, mid-ocean ridge, seafloor spreading, seismic array, seismotectonics.

1 INTRODUCTION

1.1 Geological setting

Gakkel ridge is one of the slowest spreading mid-ocean ridges worldwide; spreading rates, calculated from the model REVEL of Sella *et al.* (2002), decrease from 12.5 mm yr^{-1} (full rate) in the west at the intersection with the Lena Trough to less than 9 mm yr^{-1} near 85°E (Fig. 1) and to values of about 6 mm yr^{-1} at the eastern termination of the ridge. Global models of crustal accretion at mid-ocean ridges predict an increasing conductive heat loss of the ascending mantle at spreading rates below 15 mm yr^{-1} (e.g. Bown & White 1994). Consequently, ridges with lower spreading rates are expected to show little magmatic activity and an abnormally thin oceanic crust, its thickness decreasing with decreasing spreading rate. First gravimetric and bathymetric studies of Gakkel ridge

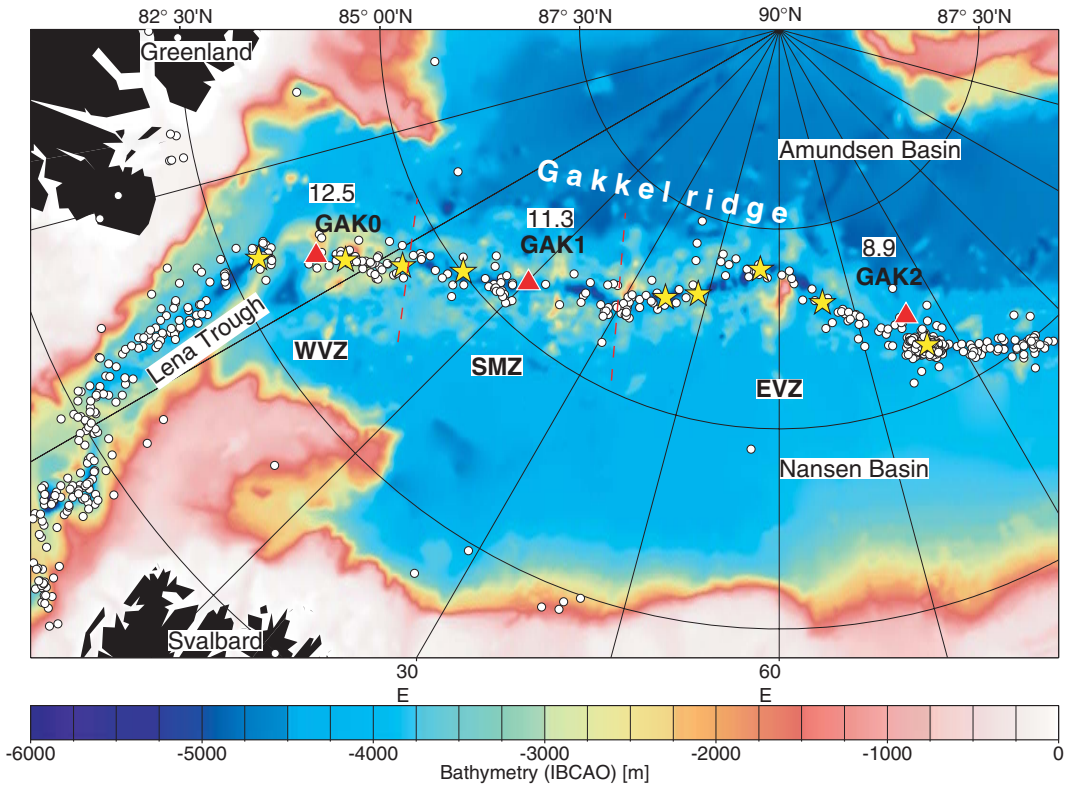

Figure 1. Location and seismicity of Gakkel ridge in the Arctic Ocean. Red triangles mark the position of the seismic arrays GAK0 in the Western Volcanic Zone (WVZ), GAK1 in the Sparsely Magmatic Zone (SMZ) and GAK2 in the Eastern Volcanic Zone (EVZ) near the large swarm of teleseismic earthquakes in 1999. White circles are earthquake epicentres (Engen *et al.* 2003; International Seismological Centre 2001). Yellow stars mark inferred hydrothermal vent fields (Edmonds *et al.* 2003). Numbers are full spreading rates in mm yr^{-1} (Sella *et al.* 2002). Bathymetry is from the International Bathymetric Chart of the Arctic Ocean (IBCAO) (Jakobsson *et al.* 2000).

gave hints on a very thin crust (Coackley & Cochran 1998; Cochran *et al.* 2003). In 2001, the international Arctic Mid-Ocean Ridge Expedition (AMORE2001) onboard the icebreakers RV *Polarstern* and USCGC *Healy* studied the bathymetry, petrological and geophysical characteristics of the crust and the hydrothermal activity of Gakkel ridge (Thiede *et al.* 2002). They found three major ridge segments with different properties (Fig. 1): the Western Volcanic Zone (WVZ) shows well-developed magmatic characteristics comparable to slow-spreading ridges despite lower spreading rates. The rift valley hosts elongate volcanic ridges, the seafloor is covered with basalts and several hydrothermal plumes were discovered (Edmonds *et al.* 2003; Michael *et al.* 2003). In contrast, the Sparsely Magmatic Zone (SMZ) shows little evidence for magmatism and a predominantly peridotitic crust. The eastern part of the SMZ and, in particular, the Eastern Volcanic Zone (EVZ) are characterized by long amagmatic rift sections and intermittent volcanic centres (Michael *et al.* 2003). The largest volcanic centre is situated near 85°E in the eastern part of Gakkel ridge (Fig. 1). Despite spreading rates of only 9 mm yr^{-1} at 85°E, it showed massive volcanic activity in 1999 with a submarine eruption (Edwards *et al.* 2001) and a swarm of teleseismically recorded earthquakes, the longest and largest of its kind (Müller & Jokat 2000; Tolstoy *et al.* 2001). AMORE2001 recovered fresh basalts from this area and detected a large hydrothermal source (Edmonds *et al.* 2003; Michael *et al.* 2003; Baker *et al.* 2004). Seismic refraction studies showed that the crustal thickness at Gakkel ridge is not a function of spreading rate as predicted, but varies with the presence or absence of volcanic centres (Jokat *et al.* 2003). All these unexpected observations lead to the definition of a new class of spreading centres, the ultraslow-spreading ridges (Dick *et al.* 2003).

The current studies yield a descriptive status quo of ultraslow-spreading ridges but no information on active processes at the rift axis, on the style of magmatism and tectonic faulting and on the mechanism of hydrothermal circulation. Microseismicity studies of other ridges have contributed considerably to understand these processes (e.g. Toomey *et al.* 1985; Sohn *et al.* 1999, 2004), and are therefore, an integrative part of a comprehensive ridge study, but they are difficult to conduct in Arctic conditions with perennial sea ice cover. In this paper, we describe a successful pilot experiment conducted during AMORE2001 to record and localize the microearthquake activity of Gakkel ridge. Despite the preliminary character of our survey, we detected magmatic and tectonic microearthquakes and the sounds of a submarine eruption (Schlindwein *et al.* 2005), all witness to active processes on the ridge.

1.2 Seismicity of Gakkel ridge

Despite its ultraslow spreading velocity, Gakkel ridge is seismically active. Engen *et al.* (2003) compiled a catalogue of teleseismically recorded earthquakes of the Gakkel ridge (Fig. 1) for the time period 1955–1999. The detection threshold of earthquakes is about Ms 3.0 at western Gakkel ridge, whereas the catalogue is considered complete for magnitudes $M_s > 4.4$. A remarkable swarm of teleseismically recorded earthquakes occurred at eastern Gakkel ridge in 1999 in relation to a submarine eruption (Müller & Jokat 2000;

Tolstoy *et al.* 2001). The earthquakes had magnitudes of 3.2–5.8. Complete coverage is expected for magnitudes $m_b > 4.5$. However, a detailed geological interpretation of the swarm is hampered by a location error of about ±10 km.

Most of the seismicity of mid-oceanic ridges occurs at magnitudes well below the completeness and detection thresholds of the Global Seismological Network. First attempts at recording the microseismicity of the Arctic mid-ocean ridge were made by Kristoffersen *et al.* (1982) in 1979 during the drift of the FRAM I ice station. They used an array of sonobuoys attached to an ice floe and successfully recorded and located about 21 regional earthquakes originating at the Gakkel ridge at a distance of 15–100 km. The earthquakes had magnitudes in the range between m_b 1 and 4. Localization was improved by using records of seismometers in northeastern Greenland and Svalbard and its accuracy is of the order of 4–10 km. Another approach was taken by Sohn & Hildebrand (2001) who used the hydroacoustic Spinnaker Array to detect earthquakes of magnitude m_b3–4 at Gakkel Ridge at a distance of 700–1000 km by means of their hydroacoustic *T*-phase, a guided acoustic wave travelling horizontally in the oceanic sound channel, an extensive layer of low sound speed. The location accuracy of this approach was of the order of tens of kilometres.

Apart from these efforts, a comprehensive study of the microseismicity of Gakkel ridge is still lacking. Such an microearthquake survey needs to achieve an epicentre accuracy of about 1 km to allow for a detailed interpretation of active tectonic and magmatic processes. This pilot study represents a feasibility study of such a microearthquake survey using a new approach with conventional land seismometers installed on ice floes.

2 EXPERIMENTAL SETUP

2.1 Survey design

Microearthquakes on mid-ocean ridges are usually detected and located with networks of ocean bottom seismometers (e.g. Toomey *et al.* 1985). Depending on the aim of the survey, a reasonable network size, instrument spacing and survey duration is chosen. The perennial sea-ice cover of the Arctic Ocean, however, prohibit such a specific survey design. Ocean bottom seismometers can not be used as the safe recovery of instruments and recorded data is hardly possible. Therefore, an entirely different experimental and methodological approach is necessary for a comprehensive study of the microearthquake activity of Gakkel ridge. After positive experience with geophones deployed on ice floes to record airgun shots (Rogenhagen & Jokat 2000), we tested in this pilot study whether conventional land seismometers installed on ice floes are able to provide high quality records of small microearthquakes.

In theory, a network of seismometers distributed over several ice floes around the potential earthquake foci provides the best localization capabilities, but it bears the unpredictable risk of loosing its sensitivity if the ice floes with the seismometers drift too far apart. We therefore, opted for an array of seismometers positioned on a single ice floe. It has the advantage of retaining its geometry and hence the array sensitivity during the drift. Fig. 2 shows the typical design of a seismological mini-array consisting of four Mark 4LC three-component short-period seismometers. The seismometers were arranged on a triangle of about 1-km-side length around a central seismometer. The equipment could be transported in one helicopter flight from the ship to the ice floe and installed in about 2–2.5 hr (Thiede *et al.* 2002). In difficult terrain, this easy installation is a major logistic advantage over for example time consuming ice floe drilling for the installation of a hydrophone array.

In order to get a first impression of the microseismicity of the different tectonic segments of Gakkel ridge, we deployed a mini-array in each of the three rift segments (Thiede *et al.* 2002). Array GAK0 operated near the rift axis in the WVZ from 2001 August 11 to 15; array GAK1 recorded the seismicity near the rift axis of the SMZ from 2001 August 20 to 24; and array GAK2 was positioned about 35 km NW of the large volcanic centre in the EVZ. This array remained in place from September 2001 2 to 13. All arrays recorded continuously at a sampling rate of 100 Hz.

The recording period of 5–11 days was determined by the logistic framework of the expedition and is not ideal for microseismicity studies. However, recording periods of several months or years can hardly be achieved in this difficult survey area. We therefore, need to bear in mind that we obtained a snapshot of the active processes at the ridge which may not be representative for geological timescales.

2.2 Array drift and GPS positioning

All array seismometers were equipped with a GPS positioning device which determined the position of the seismometer every 60 min. Fig. 2 illustrates the array drift of GAK2 by showing the seismometer positions at 4 hr intervals. The array GAK2 travelled 20 km in north–south direction and 32 km in east–west direction, but did not rotate during the drift. Array GAK1 showed minor rotation angles but in general, the sea-ice was too dense to allow rapid rotation of individual floes. We therefore, linearly interpolated the hourly GPS data to obtain the position of the array at the arrival time of each recorded earthquake. The assumption of a linear drift together with the fact that the GPS position is not logged simultaneously at all seismometers resulted in inaccurate seismometer positions. To estimate the size of this error we calculated the distance between GAK11 and GAK12 for 41 event times using interpolated GPS data and obtained an average of 1112.6 m with an rms error of 18.7 m. Considering a seismic wave travelling with a velocity of 4.5 km s^{-1} over the array, this positioning error results in a traveltime error of 0.004 s. This value is a factor of 3–10 smaller than the typical pick uncertainty of *P*-phases. We therefore, assume that the error in array positioning does not contribute significantly to the location error of earthquake epicentres in this pilot experiment.

3 CHARACTERISTICS OF THE SEISMIC SIGNALS

3.1 Identification of earthquakes

Fig. 3 shows a typical record section of the array which is band-pass filtered in the range of 8–25 Hz. The records are dominated by ice-generated noise, which is particularly evident on the horizontal component records. Seismic phases of icequakes travel horizontally in the ice floe and may have different strength at the individual seismometer sites. In contrast, signals of interest here originate below the seafloor at depths of at least 3–5 km beneath the array (Fig. 4). They travel as *P*-phases almost vertically through the water column, and therefore, show comparable signal strength on all vertical component sensors of the array with only little signal on the horizontal component records. The arrow in Fig. 3 marks a small seismic shock which fulfils these criteria. Despite high noise levels, even small earthquakes could be identified using this selection criterion. The range of waveforms of earthquakes and icequakes

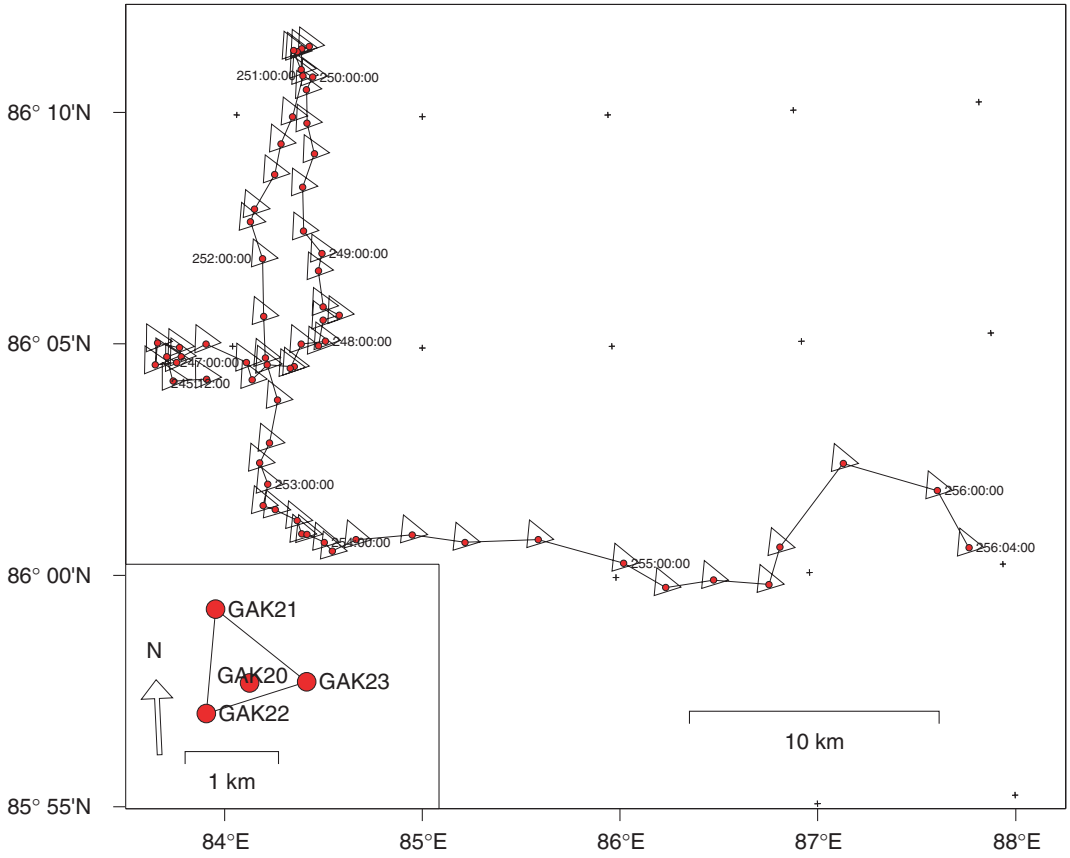

Figure 2. Drift path and geometry of the array GAK2 as determined from GPS data. The position of the array is shown at intervals of 4 hr. The numbers indicate Julian day:hour:minute. The array drifted initially eastwards, then northwards followed by a continuous southward drift. Large spacing of the array positions towards the end of the deployment period indicate a rapid eastward drift. During the drift, the orientation of the array remained stable.

varied considerably whereas both icequakes and earthquakes had similar signal frequencies. This prohibited an automated search for earthquake signals and we visually inspected all array recordings for earthquakes.

Array GAK0 detected 54 locatable events in 71 hr (0.76 events/hr), array GAK1 39 events in 87 hr (0.45 events/hr) and array GAK2 59 events in 237 hr (0.25 events/hr) and a sequence of 200 seismoacoustic events (Schlindwein *et al.* 2005). The low event rate at GAK2 results from its position 35 km north of the rift axis. Smaller earthquakes within the rift valley as observed by GAK0 and GAK1 are not detected by this array.

3.2 Waveform classification

Fig. 4 gives an overview over the waveforms recorded by the arrays. Fig. 5(a) shows the record of a teleseismic earthquake. We recorded a total of seven teleseismic events with magnitudes in the range m_b4.9–6.4. These records give a rough impression of detection sensitivity of the arrays on ice floes, but the limited number of available teleseismic records did not allow to derive, for example, delay times produced by local velocity anomalies. Fig. 5(b) shows the largest regional earthquake recorded during our experiment. Events at distances larger than about 50 km showed prominent *T*-phases which are absent for local earthquakes (Fig. 5c). Events originating in close vicinity to arrays GAK0 and GAK1 in the rift valley often showed a suite of reverberations P^1 –P^3 between sea surface and seafloor with decaying amplitudes (Fig. 5d). High acoustic impedance at the seafloor in the rift valley with upper-crustal velocities larger than 3.0 km s^{-1} (Table 1) may contribute to the effective reflection of the waves whereas the sedimentary layer underneath GAK2 appears to dampen similar reverberations from earthquakes close to GAK2.

The *SP*-phase of event 2332240 (Fig. 5d) is enclosed in the first signal package labelled *P*. A close-up is shown in Fig. 6(b) where an *SP*-phase could be identified for GAK10 and GAK13. The majority of the earthquakes either showed a short signal duration with an *SP*-phase included in the first wave package (Fig. 5d) or a long wave train with clearly discernible *P*- and *SP*-phases (Figs 5b and c). We called the short signals type A and the long signals type B.

The swarm of earthquakes in Fig. 5(e) belongs to the A-type earthquakes, however, no reverberations were recorded for these signals. The close-up in Fig. 6(a) indicates a near-vertical wave incidence with simultaneous *P*-phase onsets at all seismometers and an earthquake depth of about 5.5 km derived from the *SP*–*P* time. The swarm lasted for 23 min and consisted of 19 earthquakes, 15 of which could be localized. In contrast to typical type A and B events, the *SP*-phase of the swarm earthquakes always had lower amplitudes than the *P*-phase. This may be a mere effect of the radiation pattern of the source, but it could also point to a different source mechanism.

Swarm-like earthquake sequences were absent at GAK1, but GAK2 showed a remarkable swarm of 200 explosive events (Fig. 5f). These events, however, travelled with a velocity of about 1.5 km s^{-1} across the array and represent seismoacoustic *P* waves which propagate exclusively in the water column and not the earth's crust

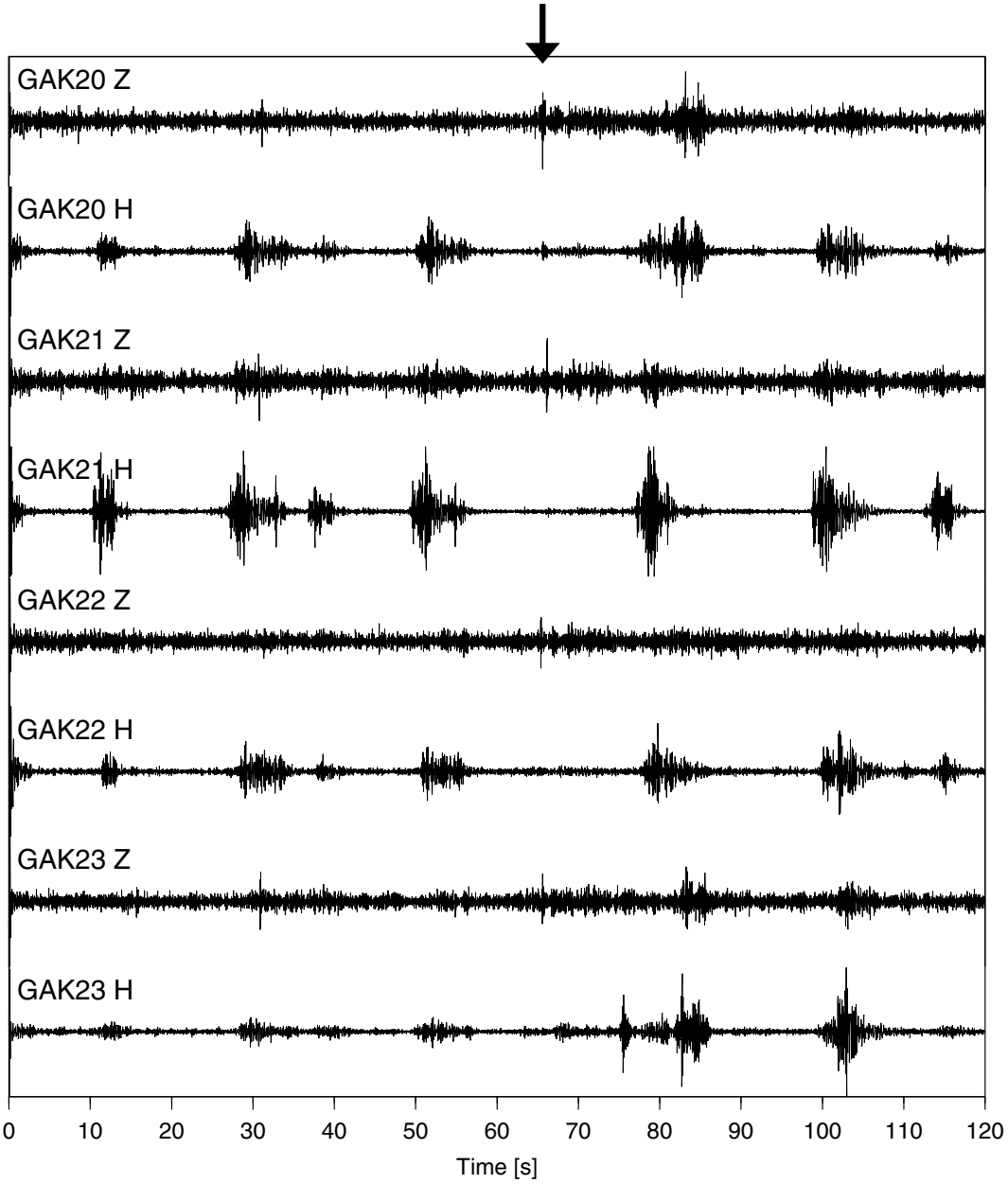

Figure 3. Example of a record section of array GAK2 (bandpass filter 8–25 Hz). For each seismometer, the vertical and one horizontal component are shown. Icequakes dominate the record section with large horizontal component signals. The arrow marks a local seismic shock which is identified by larger vertical than horizontal component signals on all array seismometers.

or mantle as all of the *P* waves of the events described so far (Figs 4 and 5a–e). The sequence of phases in Fig. 5(f) represents multiply reflected waves between the seafloor and the sea surface. In a separate study (Schlindwein *et al.* 2005), we showed that this swarm of events represents the sounds of a submarine eruption which occurred in the rift valley at a distance of about 35 km. Recordings of the water waves of repetitive airgun shots of RV *Polarstern* (Fig. 5g) show that these seismoacoustic phases can travel large distances in the Arctic Ocean without significant energy loss. The contemporaneous refraction seismic and seismological experiments during AMORE2001 (Thiede *et al.* 2002) resulted in record periods of the seismological array which are dominated by airgun shots and could, therefore, not be used to detect small local earthquakes.

3.3 Magnitudes of the recorded signals

A routine determination of the magnitude of the recorded microearthquakes is difficult in our study. The amplitudes of *P*- and *SP*-phases are modified at the interfaces rock/water and water/ice depending on the incidence angle and hence the epicentral distance of the earthquakes. In addition, it is not known how efficiently the seismometer is coupled to the ice floe. Therefore, we were unable to determine absolute amplitudes which is vital for any magnitude calculation. However, we can vaguely constrain the maximum magnitude of the recorded microearthquakes. Event 2472255 (Fig. 5b) was the largest event recorded during our survey and the most distant event. This event was too weak to be localized confidentially by the Global Seismological Network, but

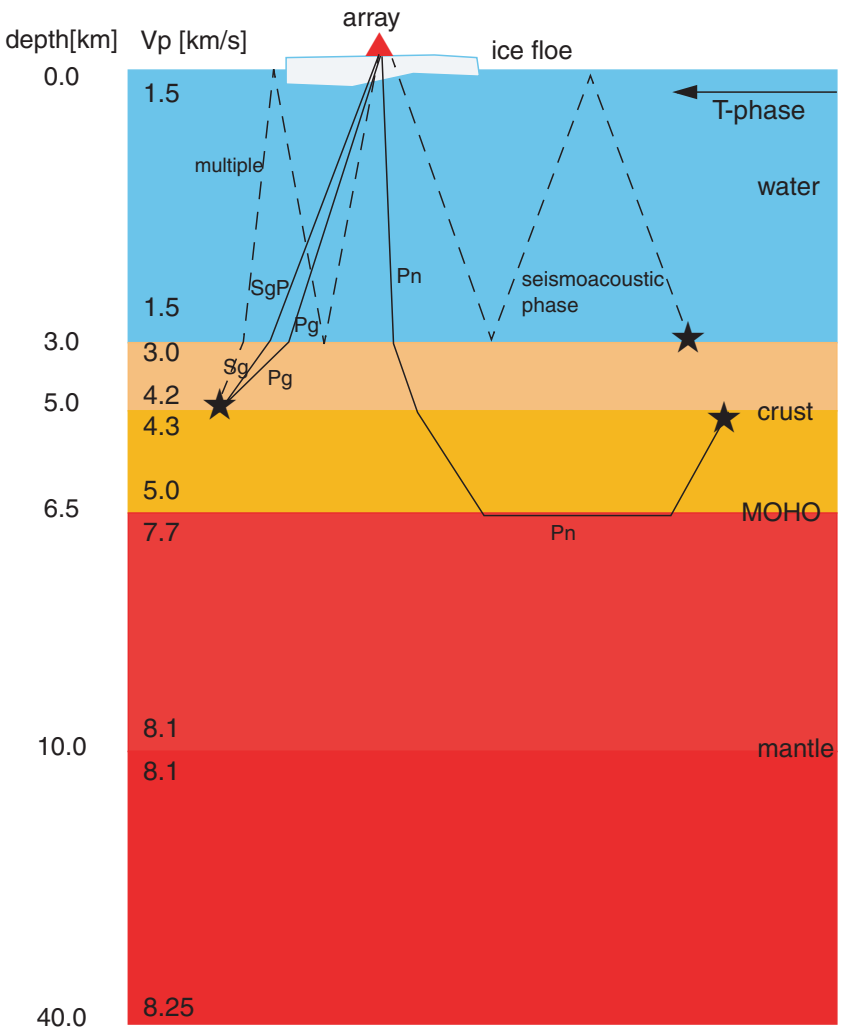

Figure 4. Schematic diagram of crustal structure and seismic phases recorded by the array. The phases are described in the text and labelled in the seismograms in Fig. 5. The velocity and depth values represent the velocity model used for array GAK0 (Table 1).

strong enough to appear in NORSAR's generalized beam forming (http://www.norsar.no/NDC/bulletins/gbf/2001/GBF01247.html), a list of fully automatic detections which are not reviewed. The quality of the automatic location and magnitude estimate of m_b2.19 is certainly poor, but it gives an upper limit for the magnitude of the recorded microearthquakes. All other events recorded in our survey had considerably smaller epicentral distances and event amplitudes, and are therefore, considered to have magnitudes well below 2.

Records of larger regional events which are well located by the Global Seismological Network could serve as calibration events in future studies and allow to determine at least relative magnitudes.

4 LOCALIZATION OF THE MICROEARTHQUAKES

4.1 Seismic velocity structure of the Gakkel ridge

Information on the seismic velocity structure of Gakkel ridge is still sparse. During AMORE2001, refraction seismic profiles were shot along the rift valley with one receiver per profile positioned on an ice floe (Jokat *et al.* 2003; Jokat & Schmidt-Aursch 2007). These data provide basic models of the crustal structure in the rift valley. However, the profiles are unreversed and crustal structure is likely to deviate from a simple 1-D model. In the absence of any other information, we derived simple 1-D velocity models for the area of GAK0 and GAK1 from nearby refraction profiles (Table 1 and Fig. 4). Depth values in this table and in the following are given in kilometres below sea surface. For the area of GAK2, no seismic profiles are available. Here, topography is subdued by a sedimentary layer which reaches a thickness of about 1 km in the rift valley near 70°E (Jokat & Micksch 2004) and 4–6.5 km further east on the ridge flank of the Nansen Basin (Kristoffersen 1990). We assumed a sediment thickness of about 2 km and an underlying crust with seismic velocities similar to those at GAK0 and GAK1 (Table 1). We first experimented with crustal thicknesses of 2.7–3.5 km plus 2 km of sediments, but obtained no convincing fit to a number of *Pg*-phases which travelled at approximate apparent velocities of 3–5 km s^{-1} across the array. A Moho depth of 11.5 km, which corresponds to a magmatic crustal thickness of about 5.7 km (Table 1), provided the best fit to the distance-dependent distribution of *Pn*- and *Pg*-phases and was used for the localization.

For each recorded event, we determined the position of the array and the water depth underneath the central array seismometer and

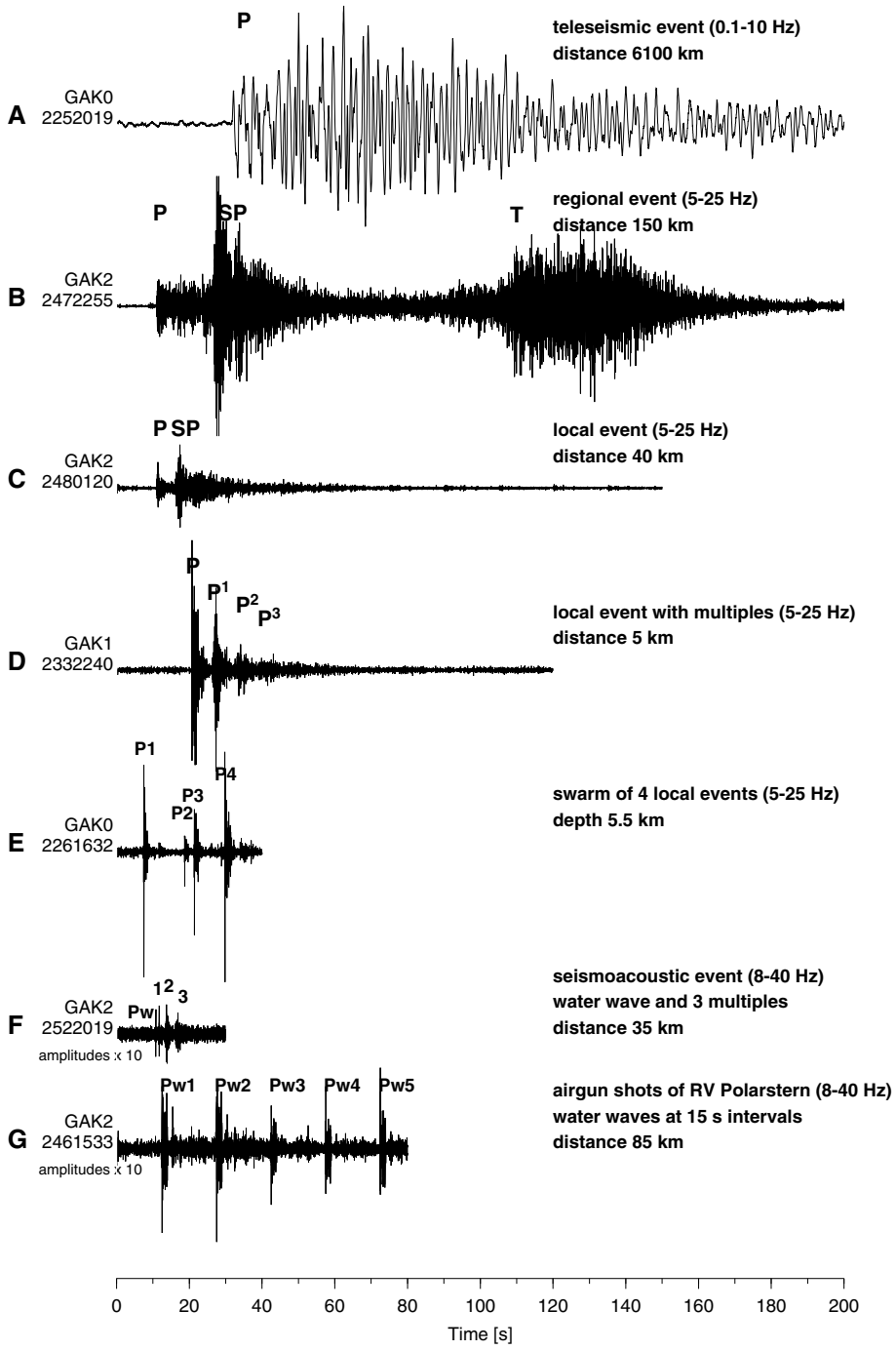

Figure 5. Types of recorded signals and identified seismic phases. Record sections of the vertical component of the indicated seismometer are shown. The frequency range of the bandpass filter is indicated. The event numbering represents Julian day, hour and minute (jjjhhmm). Note that the last two seismograms are scaled by a factor of 10. (a) Clear *P*-wave arrival of a teleseismic event. (b) Strong regional event produces a *T*-phase. This event had a magnitude of the order of 2. (c) At shorter distances, no *T* waves are generated. *P* and converted *S* wave are clearly separated phases of a long wave train (B-type event). (d) Earthquakes occurring at shallow depths close to arrays GAK0 and GAK1 produced a suite of reverberations in the water column. *P* and converted *S* wave are enclosed in the first signal package of a short waveform (A-type event). (e) Part of a swarm of 15 earthquakes beneath station GAK0. (f) and (g) These seismograms show water waves travelling exclusively in the water column with an approximate velocity of 1.5 km s^{-1} (Fig. 4). These phases can be observed over large distances. (f) Sounds of a submarine eruption (Schlindwein *et al.* 2005) and (g) Sounds of the airguns of RV *Polarstern* shooting a seismic profile.

adapted the velocity model accordingly. Hence, for the localization of each event, a specific velocity model is used which accounts for the local water depth under the array. The ice floes have an approximate average thickness of 2 m with water-saturated sponge-like structure at about 50 cm depth (Thiede *et al.* 2002), and are therefore, neglected in the velocity models.

The quality of the bathymetry data represents a further source of error in the velocity models and, hence, the event localization.

Table 1. Velocity models used for the localization of the microearthquakes. Depth values marked with * are flexible. The depth to the seafloor underneath the array is determined for the arrival time of each seismic event.

	GAK0			GAK1			GAK2		
	Depth (km)	*Vp* (km s^{-1})	*Vs* (km s^{-1})	Depth (km)	*Vp* (km s^{-1})	*Vs* (km s^{-1})	Depth (km)	*Vp* (km s^{-1})	*Vs* (km s^{-1})
Water	0.0	1.5	–	0.0	1.5	–	0.0	1.5	–
	3.0*	1.5	–	4.3*	1.5	–	3.8*	1.5	–
Crust	3.0*	3.0	1.73	4.3*	3.5	2.02	3.8*	2.0	1.16
	5.0	4.2	2.42				5.8	3.0	1.73
	5.0	4.3	2.48				5.8	3.5	2.02
	6.5	5.0	2.89	7.0	5.4	3.12	11.5	5.0	2.89
Mantle	6.5	7.7	4.45	7.0	7.4	4.50	11.5	7.7	4.45
	10.0	8.1	4.68	10.0	8.1	4.68	20.0	8.2	4.73
	40.0	8.25	4.76	40.0	8.25	4.76	40.0	8.25	4.76

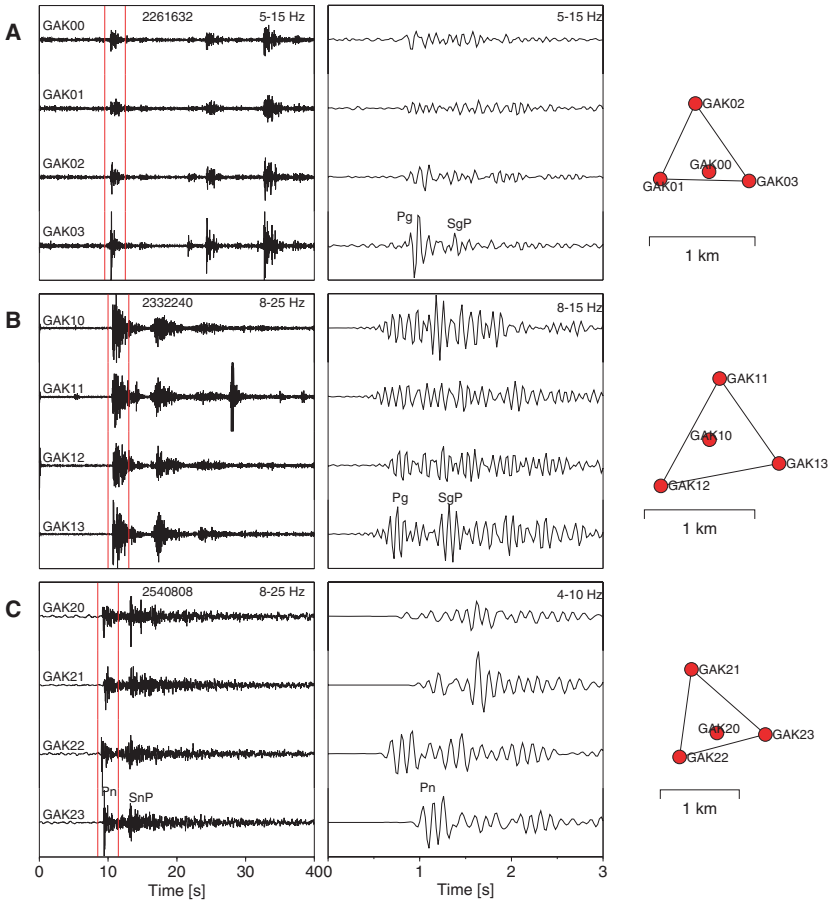

Figure 6. Example of array recordings showing the vertical component seismograms of events 2261632 (a), 2332240 (b) and 2540808 (c), along with close-ups of the signal onset between the red lines and the array orientation. (a) The events of the swarm (Fig. 5e) arrive from underneath as shown by simultaneous onset of the *Pg* phase at all seismometers. The depth to the source results from the traveltime difference of *SgP–Pg*. (b) Complicated waveform of a close-by event. Station GAK12 shows a later onset indicating an earthquake source to the northeast. (c) Coherent waveform of a regional earthquake. F–k analysis yielded a backazimuth of 210°.

High resolution bathymetry data acquired during AMORE2001 are available for the survey areas of GAK0 and GAK1. For GAK2, however, new bathymetry data are limited to a narrow track in the rift valley. Underneath the array, only IBCAO bathymetry data (Jakobsson *et al.* 2000) are available. Comparison with the newly acquired data showed that IBCAO water depths can be erroneous by several hundreds of metres which severely influences the velocity models. However, if we assume near-vertical ray incidence, an incorrect thickness of the water layer acts on all seismic phases of a recorded event in the same way and is, therefore,, unlikely to grossly distort the localization results shown below.

4.2 Localization procedure and error estimates

Locating earthquakes with a single small-aperture array is difficult and may be computationally unstable if the earthquake source is positioned outside the array. In principle, the direction of the earthquake source is determined either from backazimuths obtained from

frequency–wavenumber (f–k) analysis (Capon 1969) or from the relative onset of the phases at the array seismometers. The distance to the earthquake results from the traveltime difference between *SP*- and *P*-phase (Figs 6a–c). In the absence of any additional constraints, minor errors in both *SP–P* times and relative onsets result in erroneous distances and backazimuths and hence earthquake epicentres.

We picked *P*-phase arrival times at all four array seismometers and as many *SP*-phases as possible. For events with low-frequency *P*-phases (4–10 Hz), f–k analysis yielded backazimuth values and partly ray parameters (Fig. 6c). Events with unclear *SP*-phases or *P*-arrivals on less than four seismometers were not located. We used the inversion routine HYPOSAT (Schweitzer 2001) to calculate earthquake epicentres. The solution for each event was carefully checked. In some cases, the *P*-phases had large pick uncertainties but the sequence in which the seismometers were hit by the *P*-wave was clear. Hence, solutions were possible which fitted the onset times within their uncertainties, but not the onset sequence. In these cases, the inversion could be stabilized by providing a backazimuth estimate derived from the onset sequence.

The depth of the earthquake hypocentres could not be determined with this experimental set-up. Therefore, we localized the earthquakes with a fixed depth of 5 km below sea surface, which is in all cases within the crust. For earthquakes close to the array recognized by almost simultaneous *P*-phase arrivals at all array seismometers, the inversion becomes sensitive to hypocentral depth as the epicentral distance derived from the *SP–P* time of nearly vertically travelling *SP*- and *P*-phases defines the source depth. We thus obtained a hypocentral depth of 5.5 km for the swarm of earthquakes in immediate vicinity of array GAK0 (Fig. 6a). Whereas all earthquakes around GAK2 could be located with a fixed depth of 5 km, a depth of 6.5 km yielded the best inversion results for GAK1 except for a few earthquakes close to array GAK1 which required a depth of 5.5–6.0 km to fit the *SP–P* times (Fig. 6b). This shows that the experimental set-up allows to constrain the hypocentral depth only for earthquakes occurring more or less beneath the array. At larger epicentral distances, the solution becomes increasingly insensitive to the hypocentral depth.

The location results are shown in Figs 7–9. The error ellipses are based on the uncertainties in traveltime picks only. Inadequateness of the velocity model, misidentification of *SP*-phases and errors in the depth estimate provide further sources of mislocation. For example, a higher upper-mantle velocity will result in a shorter epicentral distance which becomes a relevant source of mislocation for distant earthquakes. We experimented with different velocity models and

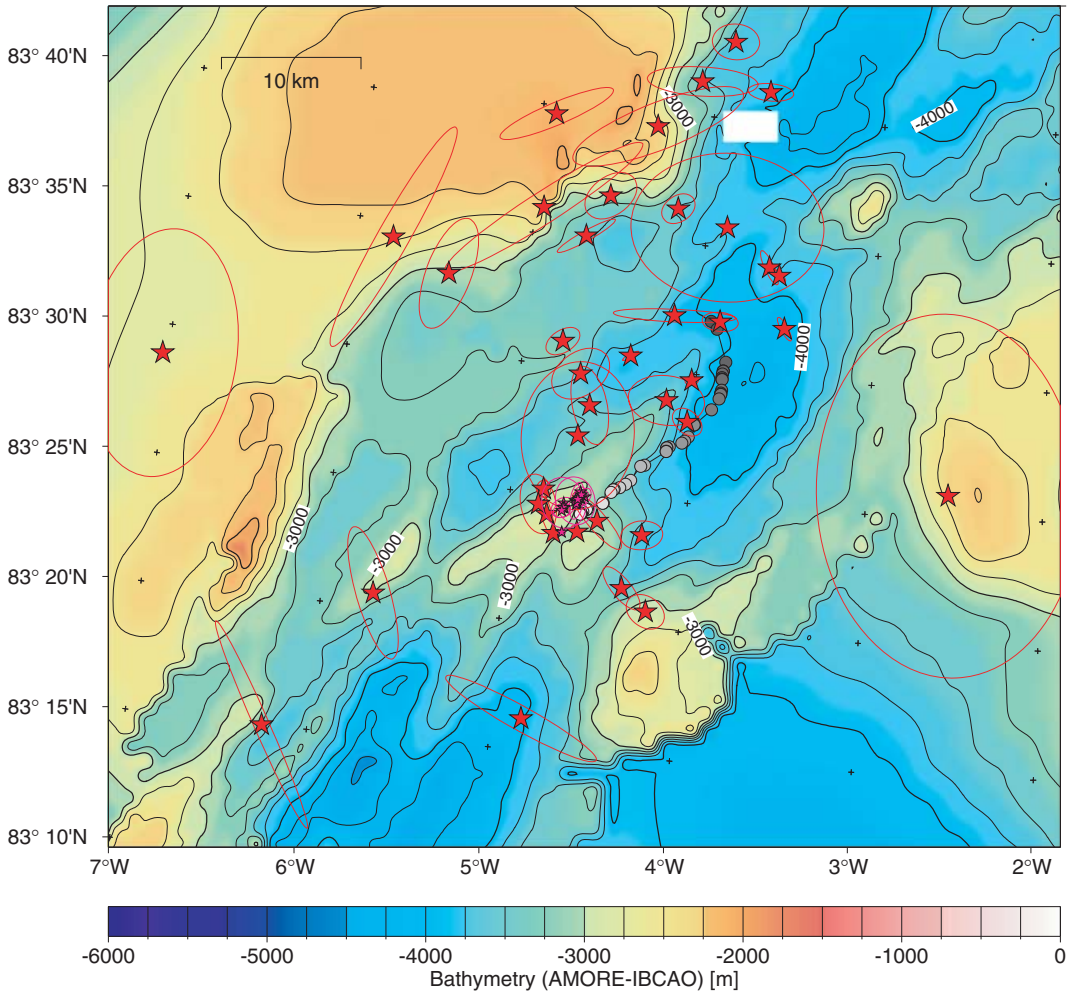

Figure 7. Earthquakes located by array GAK0 in the Western Volcanic Zone. Red stars with error ellipses indicate earthquakes of presumably tectonic origin, pink stars a swarm of volcanic earthquakes on a volcanic ridge in the central rift valley. Grey dots indicate the array positions at the time of the seismic events (drift direction from dark grey to light grey). The bathymetry grid is a combination of the more accurate data from the AMORE expedition (Thiede *et al.* 2002) in the rift valley and IBCAO data (Jakobsson *et al.* 2000) outside the rift valley. Contour interval is 250 m.

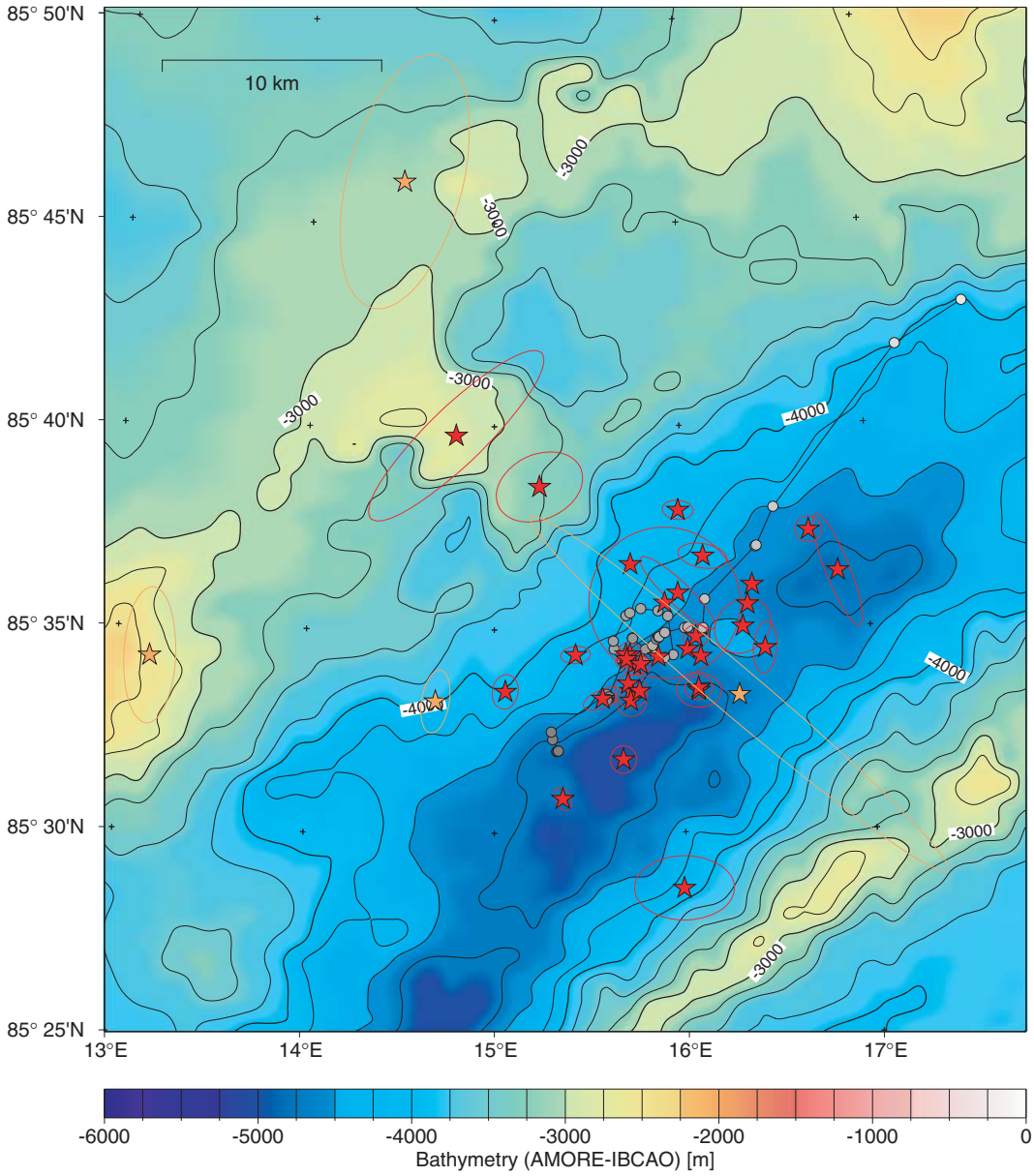

Figure 8. Earthquakes located by array GAK1 in the Sparsely Magmatic Zone. Red stars with error ellipses indicate short earthquakes with reverberations in the water column (type A, Figs 5d and 6b), orange stars local earthquakes with longer waveforms (type B, Figs 5c and 6c). The B-type earthquake in the rift valley (orange star) was recorded from the northeasternmost array position. The distinction between the earthquake types A and B is an effect of epicentral distance. See Fig. 7 for further legend.

depth values, but received a similar picture of the microearthquake distribution although not every single earthquake focus is to be found within the indicated error ellipse. The interpretation in the following chapter is, therefore, limited to statements which are supported by any of the conceivable solutions.

4.3 Results and discussion

4.3.1 Western Volcanic Zone—Array GAK0

Fig. 7 shows the epicentres of 54 recorded microearthquakes. The earthquakes were mainly of type A and B (Figs 5d and c). The former represent earthquakes originating below the rift valley floor in immediate vicinity of the array whereas the latter are located at the flanks of the mountains bounding the rift valley. The limited accuracy of the earthquake locations prevents a detailed correlation of epicentres and topographic features such as fault surfaces. However, our data support the general statement that earthquakes are preferentially connected with exposed topography like the steep escarpment at about 4.5°W 83° 35′N on the northern rift valley wall. We therefore, conclude that these earthquakes are tectonic earthquakes and signs of active faulting. Interestingly, the earthquakes are not evenly distributed: the northern rift valley wall hosts considerably more earthquakes than the southern rift valley wall although the array drifted closer to the southern wall than to the northern wall. This may point to an asymmetric spreading process. J. Snow (personal communication, 2005) counted on detailed bathymetric plots a larger number of south-facing fault escarpments on the north

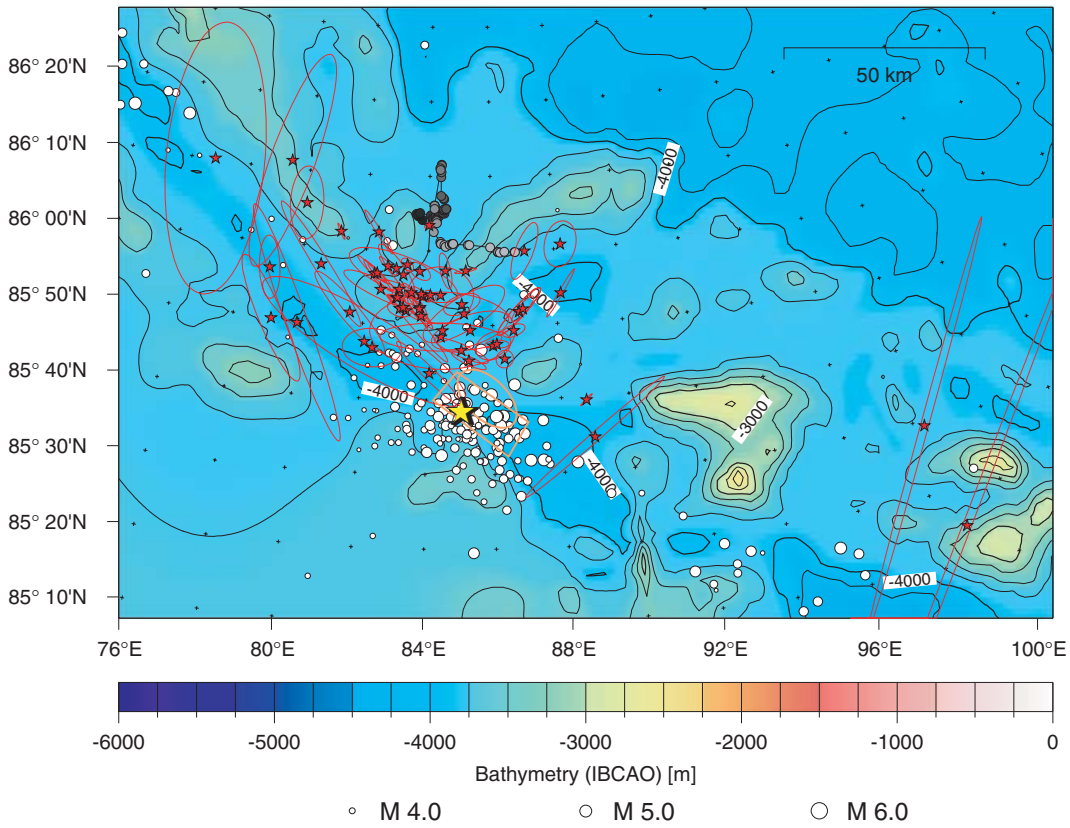

Figure 9. Earthquakes located by array GAK2 in the Eastern Volcanic Zone (red stars and error ellipses). The array drifted approximately 35 km north of the rift valley (grey dots). White circles mark the epicentres of the teleseismically recorded swarm of about 200 earthquakes in 1999 (Müller & Jokat 2000; Tolstoy *et al.* 2001), the size of the symbols is proportional to the event magnitude. The orange box delineates the area of lava erupted during the swarm in 1999 (Edwards *et al.* 2001). The yellow star marks the inferred position of a giant hydrothermal vent (Baker *et al.* 2004). The orange oval shows the source region of seismoacoustic sounds recorded in 2001 which are attributed to an active submarine eruption (Schlindwein *et al.* 2005). Bathymetry is from IBCAO data (Jakobsson *et al.* 2000) only. Contour interval is 250 m.

wall than north-facing faults on the south wall. This observation nicely matches the asymmetric distribution of microearthquakes.

Towards the end of the recording period, the array drifted over an elongate ridge in the median valley (Fig. 7). It detected a swarm of 19 earthquakes in 23 min (Figs 5e and 6a). Compared to the average event rate of 0.76 events per hour during the observation period this represents a sharp peak in seismic activity. Whereas the other events are not related in time, space or waveform characteristics, the observed swarm consists of events with very similar waveforms and phase pattern and their epicentres are clustered in time and space. Due to the proximity of the array, 15 of these earthquakes could be located with high accuracy about 2.5 km beneath the ridge crest. The earthquake swarm does not have the appearance of a typical main shock–aftershock sequence, but a rather random distribution of event amplitudes. Signal shapes differ from A-type events observed in the vicinity by a lack of reverberations and small amplitudes of the *SP* phases. We therefore, speculate that this swarm of microearthquakes is of magmatic rather than tectonic origin although a more rigorous distinction is not possible with this pilot study. Michael *et al.* (2003) described this ridge as volcanic edifice and recovered fresh basalts from several locations along the ridge. The swarm of earthquakes may thus yield evidence for active magmatism in the WVZ and may result from active hydrothermal venting, motion of magma or fluids at depth or similar processes which have not a purely tectonic origin.

4.3.2 Sparsely Magmatic Zone—Array GAK1

Seafloor spreading in the SMZ appears to be amagmatic. Apart from two volcanic centres at 13°E and 19°E, the seafloor is covered by peridotites rather than basalts and volcanic topographic features are absent (Michael *et al.* 2003). Array GAK1 drifted between these two volcanic centres in an amagmatic section of the rift (Fig. 8). However, the rift valley is seismically active. The array detected 39 events of type A and B, but no earthquake swarms. Whereas for array GAK0, A-type earthquakes could be attributed to the rift valley and B-types earthquakes to the rift flanks, it becomes evident here, that this distinction is a mere effect of epicentral distance. Two A-type earthquakes originate from the rift flanks and were recorded when the array drifted close the northern rift flank. Vice versa, a B-type earthquake with a likely epicentre in the rift valley was detected at the end of the recording period when the array was at about 20 km distance to the northeast.

Although less evident than in the WVZ, a correlation of exposed topography and earthquakes epicentres and the same asymmetric distribution of seismicity can be seen here. We attribute the seismicity of the rift valley to active tectonism.

4.3.3 Eastern Volcanic Zone—Array GAK2

Array GAK2 was installed about 35 km northwest of the large volcanic centre in the EVZ. Fig. 9 shows the swarm of teleseismically

recorded earthquakes of 1999 and the associated lava flow. The array detected 59 local and regional earthquakes, but no seismicity near the volcanic centre in the rift valley. Most of the microearthquakes occurred between the rift valley and the array positioned 35 km off-axis, but about 10 events had larger epicentral distances. The most distant event at about 98°E (Fig. 5b) had an estimated magnitude of about 2. Hence, the array may not have recorded low-level seismicity at the volcanic centre, but it certainly had the capability to detect events of magnitude 2 or even below. The absence of such events from the centre of volcanic activity of 1999 suggests that the swarm activity of 1999 may have ceased at least during our observation period. However, we detected a swarm of seismoacoustic signals which originate near this volcanic centre (Fig. 9). These signals are interpreted to be the sounds of an ongoing submarine eruption (Schlindwein *et al.* 2005). Unlike the eruption in 1999, our microearthquake survey shows that this new eruption is evidently occurring seismically silent as it is not connected with increased seismicity in number and strength of earthquakes. Further support of active volcanism comes from the detection of a massive hydrothermal plume over the volcanic centre during AMORE2001 and the recovery of fresh basalts (Edmonds *et al.* 2003; Michael *et al.* 2003; Baker *et al.* 2004).

Whereas the detection capabilities of the array are certainly limited in the median valley at 35 km distance, any seismicity immediately north of the array would have been detected (Fig. 9). During 11 days of recording no earthquake occurred here whereas 59 earthquakes were recorded in the same time period nearer to the rift axis. We can therefore, speculate that the crust in this area is currently undergoing brittle deformation out to a distance of about 30–35 km off-axis where the seismicity appears to die off. This may not apply to other ridge segments of Gakkel ridge, since GAK2 is situated in the vicinity of a large volcanic centre and *Pg–Pn* crossover distances of the seismic events point to a Moho depth of roughly 11.5 km compared to depths of about 7 km or less elsewhere (Table 1). Whereas the earthquake data can only give a rough estimate of the Moho depth, it appears likely in the light of the refraction seismic and petrologic data (Jokat *et al.* 2003; Michael *et al.* 2003; Jokat & Schmidt-Aursch 2006) that the basaltic layer of the crust may have a strongly increased thickness in vicinity of this massive volcanic centre.

5 CONCLUSIONS

Our microearthquake study of Gakkel ridge had the character of a pilot experiment. In view of future systematic seismicity studies of Gakkel ridge we can draw the following conclusions.

(1) Ice floes are suitable platforms for seismometers: despite high levels of noise connected with the movement of the ice floes, microearthquakes of magnitudes well below 2 can be detected and localized. Seismological arrays, installed on a single ice floe, retain their detection sensitivity during the ice drift, whereas networks of seismometers installed on several ice floes may loose their sensitivity. A network of several arrays would improve localization capabilities and decrease location errors in future surveys. Simultaneous GPS position logging at all seismometers of one array at intervals of about 10 min reduces positioning errors of the array during times of rapid ice drift.

(2) Despite the limited detection and localization capabilities of our pilot experiment, a meaningful geological interpretation of the recorded seismic events was possible. We were able to characterize and localize several types of microearthquakes which give a first impression of the microseismicity of Gakkel ridge. Most of the seismicity shows signs of typical tectonic earthquakes, and may therefore, point to active faulting in the rift valley and the adjacent rift mountains which appears to be asymmetric at western Gakkel ridge. A swarm-like sequence of earthquakes over a volcanic ridge at western Gakkel ridge is speculated to be of magmatic origin as well as a swarm of 200 seismoacoustic events recorded near a volcanic centre at eastern Gakkel ridge (Schlindwein *et al.* 2005).

(3) The pilot study yielded encouraging results for a future systematic analysis of the microseismicity of Gakkel ridge. An improved survey design with several seismological arrays recording simultaneously over time periods of at least 14 days would record a sufficiently large number of earthquakes to allow for a comparison of seismicity levels between ridge segments. In addition, localization uncertainties could be reduced and focal depth and mechanisms better constrained. A carefully designed follow-up microearthquake survey of Gakkel ridge may hence address the question why volcanism at ultraslow-spreading ridges is focused in individual centres and how crustal accretion works in these volcanic centres compared to amagmatic rift sections.

ACKNOWLEDGMENTS

We thank the officers and crews of RV *Polarstern* and USCGC *Healy* for their technical and logistical support, and the helicopter teams and all the members of the AMORE scientific party for their efforts. This work was funded by the Deutsche Forschungsgemeinschaft grant JO191/6-1.

REFERENCES

Baker, E.T. *et al.*, 2004. Hydrothermal venting in magma deserts: the ultraslow-spreading Gakkel and Southwest Indian Ridges, *Geochem. Geophys. Geosyst.,* **5,** Q08002, doi:10.1029/2004GC000712.

Bown, J.W. & White, R.S., 1994. Variation with spreading rate of oceanic crustal thickness and geochemistry, *Earth planet. Sci. Lett.,* **121,** 435–449.

Capon, J., 1969. High-resolution frequency-wavenumber spectrum analysis, *Proc. IEEE,* **57,** 1408–1418.

Coackley, B.J. & Cochran, J.R., 1998. Gravity evidence of very thin crust at the Gakkel Ridge (Arctic Ocean), *Earth planet. Sci. Lett.,* **162,** 81–95.

Cochran, J.R., Kurras, G.J., Edwards, M.H. & Coackley, B.J., 2003. The Gakkel Ridge: bathymetry, gravity anomalies, and crustal accretion at extremely slow spreading rates, *J. geophys. Res.,* **108**(B2), 2116, doi:10.1029/2002JB001830.

Dick, H.J.B., Lin, J. & Schouten, H., 2003. An ultraslow-spreading class of ocean ridge, *Nature,* **426,** 405–412.

Edmonds, H.N. et al., 2003. Discovery of abundant hydrothermal venting on the ultraslow-spreading Gakkel Ridge in the Arctic Ocean, *Nature,* **421,** 252–256.

Edwards, M.H., Kurras, G.J., Tolstoy, M., Bohnenstiehl, D.R., Coackley, B.J. & Cochran, J.R., 2001. Evidence of recent volcanic activity on the ultraslow-spreading Gakkel Ridge, *Nature,* **409,** 808–812.

Engen, Ø., Eldholm, O. & Bungum, H., 2003. The Arctic plate boundary, *J. geophys. Res.,* **108**(B2), 2075, doi:10.1029/2002JB001809.

International Seismological Centre, 2001. On-line Bulletin, http://www.isc.ac.uk/Bull, Internatl. Seis. Cent., Thatcham, United Kingdom.

Jakobsson, M., Cherkis, N.Z., Woodward, J., Macnab, R. & Coackley, B., 2000. New grid of Arctic bathymetry aids scientists and mapmakers, *EOS, Trans. Am. geophys. Un.,* **81,** 89, 93, 96.

Jokat, W. & Micksch, U., 2004. Sedimentary structure of the Nansen and Amundsen basins, Arctic Ocean, *Geophys. Res. Lett.,* **31,** L02603, doi:10.1029/2003GL018352.

Jokat, W. & Schmidt-Aursch, M.C., 2007. Geophysical characteristics of the ultra-slow spreading Gakkel Ridge, Arctic Ocean, *Geophys. J. Int.,* in press.

Jokat, W., Ritzmann, O., Schmidt-Aursch, M.C., Drachev, S., Gauger, S. & Snow, J., 2003. Geophysical evidence for reduced melt production on the Arctic ultraslow Gakkel mid-ocean ridge, *Nature,* **423,** 962–965.

Kristoffersen, Y., 1990. Eurasia Basin, in *The Geology of North America, Vol. L, The Arctic Ocean Region*, pp. 365–378, eds Grantz, A., Johnson, L. & Sweeney, J. F., Geol. Soc. Am., Boulder, Colorado.

Kristoffersen, Y., Husebye, E.S., Bungum, H. & Gregersen, S., 1982. Seismic investigations of the Nansen ridge during the Fram I experiment, *Tectonophysics,* **82,** 57–68.

Michael, P.J. *et al.*, 2003. Magmatic and amagmatic seafloor generation at the ultraslow-spreading Gakkel Ridge, Arctic Ocean, *Nature,* **423,** 956–961.

Müller, C. & Jokat, W., 2000. Seismic evidence for volcanic activity discovered in Central Arctic, *EOS, Trans. Am. geophys. Un.,* **81**(24), 265+269.

Rogenhagen, J. & Jokat, W., 2000. The sedimentary structure in the western Weddell Sea, *Mar. Geol.,* **128,** 45–60.

Schlindwein, V., Müller, C. & Jokat, W., 2005. Seismoacoustic evidence for volcanic activity on the ultraslow-spreading Gakkel Ridge, Arctic Ocean, *Geophys. Res. Lett.,* **32,** L18306, doi:10.1029/2005GL023767.

Schweitzer, J., 2001. HYPOSAT—an enhanced routine to locate seismic events, *Pure appl. geophys.,* **158,** 277–289.

Sella, G.F., Dixon, T.H. & Mao, A., 2002. REVEL: a model for recent plate velocities from space geodesy, *J. geophys. Res.,* **107**(B4), 2081, doi: 10.1029/2000JB000033.

Sohn, R.A. & Hildebrand, J.A., 2001. Hydroacoustic earthquake detection in the Arctic Basin with the Spinnaker Array, *Bull. seism. Soc. Am.,* **91**(3), 572–579.

Sohn, R.A., Hildebrand, J.A. & Webb, S.C., 1999. A microearthquake survey of the high-temperature vent fields on the volcanically active East Pacific Rise (9°50′N), *J. geophys. Res.,* **104**(B11), 25 367–25 377.

Sohn, R.A., Barclay, A.H. & Webb, S.C., 2004. Microearthquake patterns following the 1998 eruption of Axial Volcano, Juan de Fuca Ridge: mechanical relaxation and thermal strain, *J. geophys. Res.,* **109,** B01101, doi:10.1029/2003JB002499.

Thiede, J. & the shipboard scientific party, 2002. Cruise Report: AMORE2001, *Rep. Polar Mar. Res.*, **421,** 397 pp.

Tolstoy, M., Bohnenstiehl, D.R., Edwards, M.H. & Kurras, G.J., 2001. Seismic character of volcanic activity at the ultraslow-spreading Gakkel Ridge, *Geology,* **29,** 1139–1142.

Toomey, D.R., Solomon, S.C., Purdy, G.M. & Murray, M.H., 1985. Microearthquakes beneath the median valley of the Mid-Atlantic Ridge near 23°N: hypocenters and focal mechanisms, *J. geophys. Res.,* **90**(B7), 5443–5458.